JOURNAL OF OPTOELECTRONICS AND ADVANCED MATERIALS Vol. 8, No. 4, August 2006, p. 1479 - 1483

High porosity sintered sheets

I. VIDA - SIMITI
Technical University of Cluj-Napoca, 3400-Cluj-Napoca, Romania

The sintered sheets having high porosity were obtained from metallic and ceramic powders by free spreading methods followed by sintering. The sintered structure consists of the framework of the basic metals (metallic matrix) and the spatial network of pores. The relations between the mechanical characteristics and the porosity are determined. The fracture mechanism suggested by scanning electronic microscopy studies is described. The rolling with elastic cylinder allows the bending sintered sheets having a low curvature radius.

(Received March 14, 2006; accepted July 20, 2006)

Keywords: Sintered materials, Porosity, Porous materials

1. Introduction

The porous materials obtained in layers by free spreading, compaction and sintering metallic and ceramic powders are used as a semi product to obtain filtering elements of different geometrical forms through plastic deformation, welding and machining. The specific structure of these materials consists of a metallic framework formed by particles of sintered powder and a spatial lattice of pores, most of them opened and interconnected with one another. Interconnected pores ensure a good permeability [1-3]. Many studies analysed the dependence of mechanical properties with porosity in the case of sintered iron [4-8]

In the present report we analyse the influence of porosity and powder sizes on tensile strength, compression and yield limit of sintered sheets made by stainless steel. We analyse the influence of compacting pressure on porosity, pore sizes and permeability of sintered sheets. Since of porous structure, the bending of sintered sheets was performed by a rolling method using an elastic cylinder [9].

2. Sample preparation and experimental methods

The stainless steel powder used in the present report has the composition (wt%) 0.3 C, 16…18 Cr, 10…12 Ni and Mo, 1 Si, 0.03 S, 0.03 P, the remainder being Fe. Three ranges of particle sizes were used: < 40 μm, 40 – 80 μm, 80 – 125 μm. The homogenized powder was strewn on a steel sheet-metal used as a support. The support plates are isolated on both sides by covering them with a fine-grained Al_2O_3 layer. The powder layer is then dressed at the desired thickness (1…2 mm). By sintering porous sheets having 1.5 mm thickness were obtained.

Sintering has been performed in a hydrogen atmosphere, at (1290 – 1310) ºC during 120 min. The tensile strength and the conventional yield limit were determined by using an universal testing equipment "Instron" type.

The elastic cylinder method was used for bending the porous sheets (Fig. 1). The equipment consists of two cylinders having different diameters, one rigid and the second elastic. The curvature of sheet depends on the pressing force F, on the depth of penetration H_0 in the elastic layer, respectively.

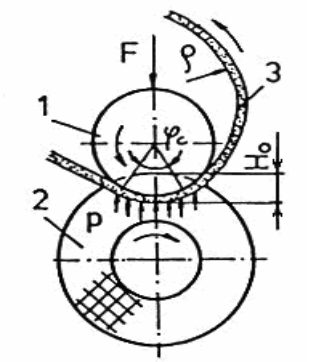

Fig. 1. The diagram of the rolling of sintered porous sheets.

3. Mechanical properties

The shape of the sample used for determining mechanical properties is shown in Fig. 2. This ensures the fracture in the central area at the minimum width area respectively [7].

The dependences of the tensile strengths and yield limits on the porosities for different particles sizes are plotted in Figs. 2a. and 2b. Both tensile strengths, R_p, and yield limits, R_{p02}, decrease with increasing porosity. The variations are higher in case of powder having smaller sizes. The best fit of the experimental data was obtained by using an exponential function described by the relation [10]:

$$R_p = R_m \times \exp(-V_1 P) \quad (1)$$

where R_m is the tensile strength of the material compact powder matrix, P is the porosity; $V_1 = 5.13$ for the particle

sizes < 40 μm; 5.86 for the particle size (40-80) μm and 6.63 for the particle sizes (80-125) μm.

The parameter V_1 represents the decreasing rate of the tensile strength with increasing porosity. From the data given above, one can see that V_1 increases linearly with the increasing granulation of the powder used. Therefore the tensile strength of the sheet metals decreases.

If we consider all the powder particle size ranges, the dependence of the tensile strength on the porosity is more complicated, being described by the relation:

$$R_p = R_m(1-P^2)^2 \times \exp(-V_2 P) \qquad (2)$$

where: $V_2 = 4.49$.

The dependence of yield limit, R_{p02}, on porosity is also described by the relation (2). The V_2 parameters are dependent on the particle sizes: $V_2 = 2.27$ for the particle size < 40 μm; 3.48 for the particle size (40-80) μm; 4.39 for the particle size (80-125) μm; and 3.12 in all the range of sizes.

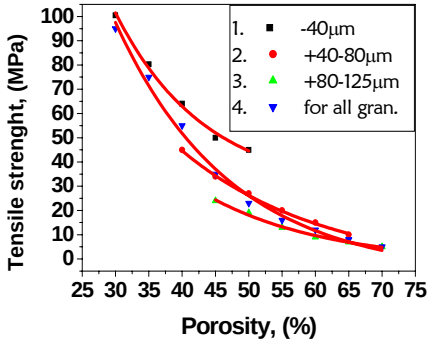

a

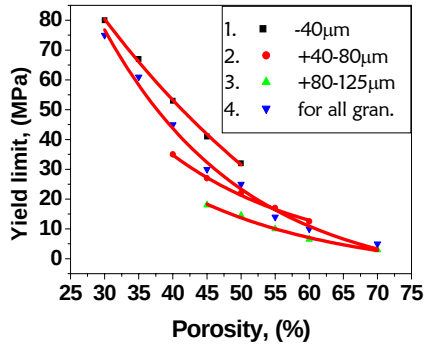

b

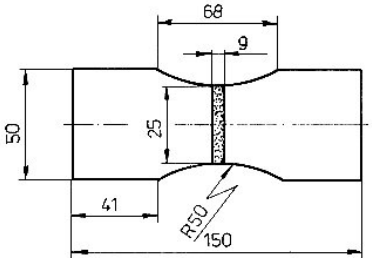

c

Fig. 2. Dependence of tensile strength (a) and of yield limit (b) on porosity for different particle sizes, (c) sample used for tensile test.

The scanning electron microscopy analysis of the fracture surfaces of the porous sheet subjected to traction stress shows that the fracture zone is localized in the necks generated by sintering (Fig. 3). These necks are concentration zones of the tensions that determine the fracture as well as the propagation of the cracks. The fractures take place after well marked plastic deformations of the sintering neck. The presence of the sliding planes on some fractured necks was also shown. This justifies the moderately ductile character of the necks fracture, which can be correlated with the austenitic structure of the metallic matrix. In case of the porous material assembly, the fracture of the porous component is similar as that characteristic for a brittle system.

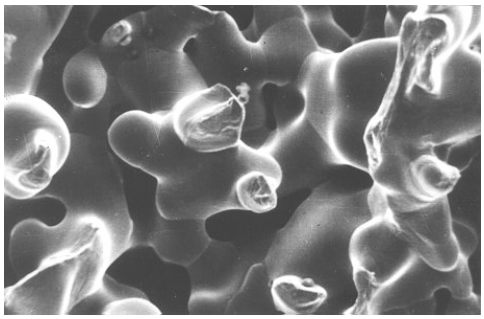

a

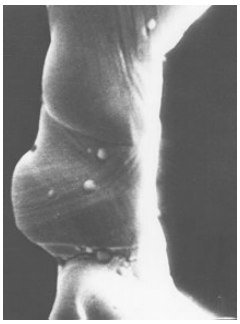

b

c

Fig. 3. SEM images of the fracture: a - general view (x1000), b – elongated sintering neck (x10000), c – fractured neck (x10000).

Compression tests of samples having different initial thicknesses and porosities were carried out by using an

Instron type equipement. The punch diameter was 11.3 mm. During each loading step, the load (as well as the respective pressure) has been determined by using the relation:

$$\varepsilon = \ln \frac{h_0}{h} \tag{3}$$

where h_0 is the initial thickness of the sheet and h is the thickness after deformation.

The characteristics plots: pressure – plastic deformation, p=f(ε), porosity – pressure, P=f(p), and porosity – plastic deformation, P=f(ε), Figs. 4-6, can be described by the exponential relations (4 -6).

$$p = A \cdot \exp(B \cdot \varepsilon) \tag{4}$$

$$P = P_o \cdot \exp(C \cdot p) \tag{5}$$

$$P = 1 - (1 - P_0) \cdot \exp(M \cdot \varepsilon) \tag{6}$$

The A, B, C and M parameters where determined by computer fitting of experimental data and are given below the figures.

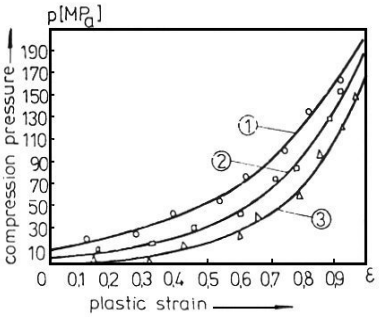

① p = 13 exp(2,8 ε); P_o = 46 % ③ p = 1,6exp(4,7 ε); P_o = 63 %
② p = 5,3exp(3,6 ε); P_o = 55 %

Fig. 4. Compression - strain curves.

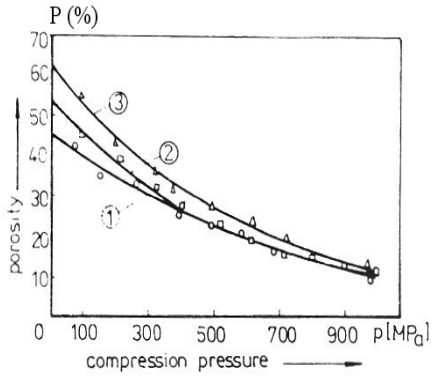

① P = $P_o$exp(–0,015 p); P_o = 46 % ③ P = $P_o$exp(–0,017 p); P_o = 63 %
② P = $P_o$exp(–0,018 p); P_o = 55 %

Fig. 5. Pressure dependence of the porosity.

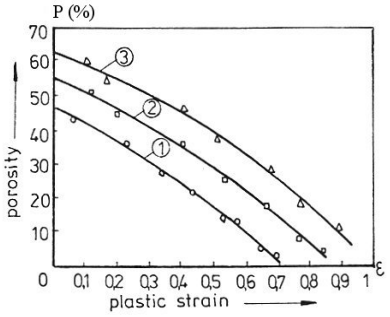

① P = 1–(1– P_o)exp 0,87 ε; P_o = 46 % ③ P = 1–(1– P_o)exp ε; P_o = 63 %
② P = 1–(1– P_o)exp 0,92 ε; P_o = 55 %

Fig. 6. Dependence of the porosity on the plastic strain.

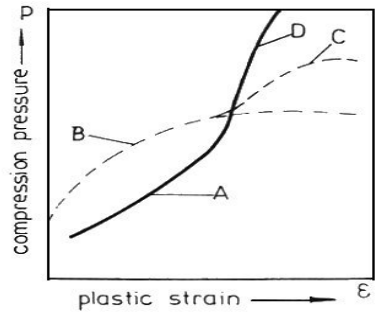

Fig. 7. - Characteristic shapes of strain curves: A+D – porous sintered sheet; B – compact material; C – sintered material with reduced porosity.

The compression deformation characteristics of the sintered porous sheets having high porosity (curve A) are different from those of the compact sintered materials (curve C) and of the sintered materials having a low initial porosity (Curve B in Fig. 7). The above behavior may be explained by the decrease of the porosity after compression.

When the complete compaction is achieved, theoretically the material tends to behave like as a compact body (Fig. 7 curve C). A well-marked increase of the pressure determines a small increase of deformations (curve D) till the complete crushing of the material under the punch takes place. The differences in shape between the curves C and D may by explained by a well-marked strain hardness of the metallic matrix, as well as by deformation and compaction in the region with low plastic strain.

4. Structure and permeability of sintered porous sheets

In order to determine the maximum size of pores, the bubble test was used according to the methodology provided by the international standard EN 24003. From the above mentioned samples, disks having a 60 mm diameter and about 3 mm thicknesses were prepared. For this study, four range of particle sizes were used: < 50 μm, 50 – 71 μm, 71 – 100 μm and 100 – 160 μm. The influence of the compacting pressure on the porosity is

presented in Fig 8a. A marked decrease of porosity particularly for powder having small sizes was shown.

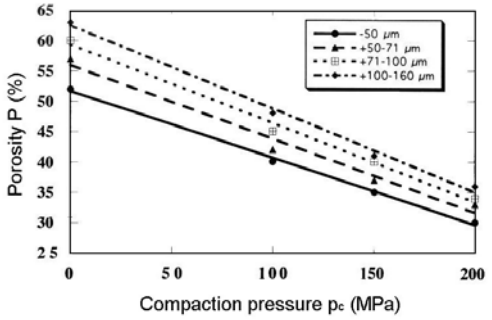

a

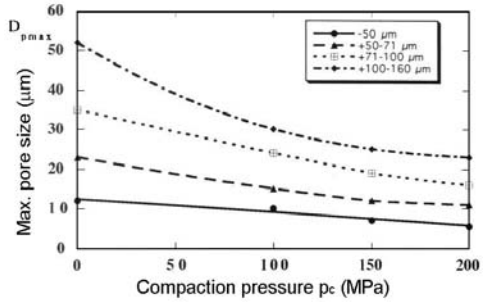

b

Fig. 8. Influence of compacting pressures on porosities (a) and pore sizes (b).

The influence of the compacting pressure on the pore maximum sizes for different particle size range is shown in Fig. 8b. The maximum size of the pores increases with the increase of the powder particle sizes. The above behavior is explained by the different sizes of the empty spaces left in the arrangement of the compacted particles.

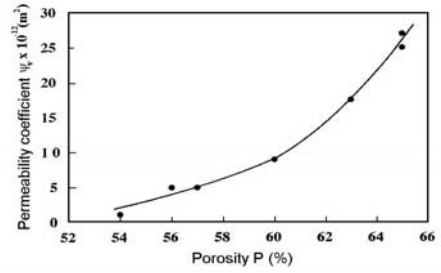

a

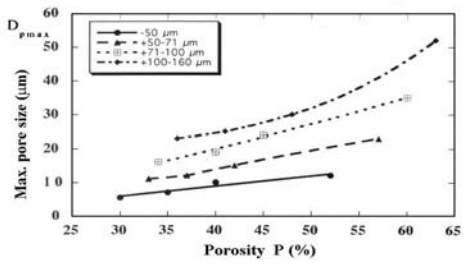

b

Fig. 9. Variation of the permeability coefficient (a) and maximum pore size (b) as function of porosity.

The influences of the porosity on the viscous permeability coefficient (a) and the maximum pore size (b) in the case of air flow through the pores are given in Fig. 9. The porosity is determined by compacting pressure and powder sizes.

5. Surface effect

In the case of thin sintered sheets obtained from powders, there is a thickness dependence of structural and functional parameters. From a certain thickness, depending on the powder sizes, there is an uniform porous structure which ensures the reproductibility of the parameters and functional characteristics. As the superficial layers of the sheets have reduced densities, and consequently higher porosities compared to the rest of the porous body, the above surface effect manifests its influence in the case of thin sheets. Thus, the lower porosity of the superficial layers influences the porosity of the porous body as a whole. The effect is more marked in the case of sheets obtained from powder having greater particle sizes. For a certain thickness the surface effect disappears. The porosity and the maximum pore diameter, $D_{p\ max\ e}$, as function of sheet thickness are presented in Fig. 10. For higher thickness than a characteristic value, denoted by broken line, the maximum pore dimensions are not dependent on thickness. The $D_{p\ max\ e}$ values obtained in this region (zone I in Fig. 10 b) for different particles areas are listed in Table 1.

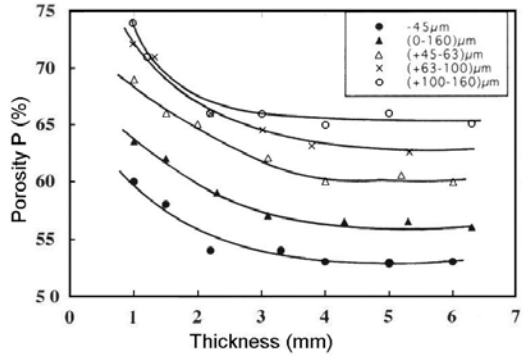

a

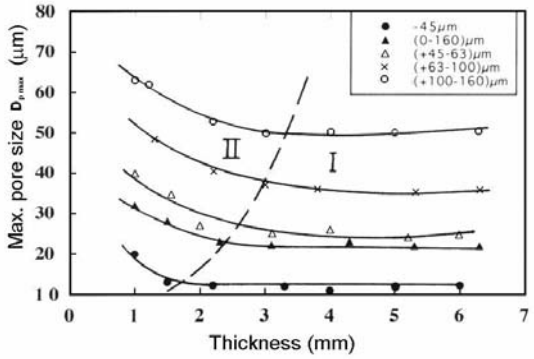

b

Fig. 10. Variation of porosity (a) and maximum pore size (b) as function of the thickness of the porous sheet.

Table 1. Critical thickness and equalling diameter.

Size range	45 [μm]	0-160 [μm]	45-63 [μm]	63-100 [μm]	100-160 [μm]
Sheet thickness [mm]	1.5	2	2.5	2.8	3.0
$D_{p\ max.e}$ [μm]	12.3	22	25	36	50

This region corresponding to higher thickness, characterizes the ordered, regular porous structures, while zone II to the irregular structures (Fig. 10).

6. Rolling of sintered sheets

The influences of pressing force F and penetration H on the relative radius of curvature were also studied. When increasing the pressing force, a diminution of the bending relative radius is noted. This variation is explained by the greater contact angle φ_c, between the roller 1 (Fig.1) and the porous sheet, so the modelling effect becomes stronger. The dependence of the curvature relative radius versus the pressing force and the depth of penetration respectively can be described by exponential relations:

$$\rho_{rel} = A_1 \cdot \exp(-B_1 F) \quad (7)$$

$$\rho_{rel} = A_2 \cdot \exp(-B_2 H) \quad (8)$$

where: A_i, B_i parameters were determined by fitting the experimental data (insert in figures).

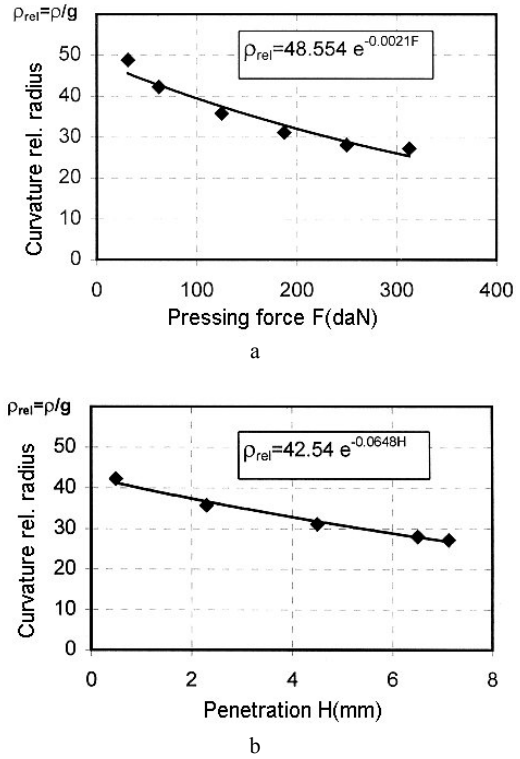

Fig. 11. Influence of the pressing force (a) and penetration (b) upon on the curvature relative radius.

We note that the data from Fig. 11 are mean values obtained from different experiments.

7. Conclusions

The dependences of the mechanical characteristics as a function of the sheet porosity of stainless metallic powder having high porosity have an exponential form. Both the tensile strength and yield limits decrease when increasing porosity. The fracture zone is localised in the necks generated during sintering process. The necks are concentration zones of tension that determine fracture and constitute a propagation region for the cracks.

The influence of rolling process on the porous characteristics was also analysed. The curvature radius follows an exponential dependence on the pressing force. The rolling radius (deformability indices) depends on the thickness and porosity of the structure and represent and indicator of the deforming capacity.

For each particle size ranges used, there are porosity variations at reduced thickness of the samples, due to the surface effect. A critical thickness of the porous permeable layers is found, from which the maximum pore dimension remains constant.

References

[1] W. Schatt, K. P. Wieters - Powder Metallurgy. Processing and Materials, EPMA, (1997).
[2] Albano-Müller, Powder Metallurgy International **14**, 73 (1982).
[3] G. A Wilson, - Porous Metal Filters. Selected Case Studies in PM, The Institute of Metals Series on PM, London, p. 76 (1991).
[4] S. V. Belov, Porous Metals in Mechanical Engineering, Moskow, 1981.
[5] H. Danninger, G. Jangg, B. Weiss, R. Stickler, Powder Metallurgy **25,** 111 (1993).
[6] G. F. Bocchini, Int. J. Powder Metallurgy. **22**, 185 (1986).
[7] B. Karlsson, I. Bertilsson, Scand. J. Metallurgy **11**, 267 (1982).
[8] A. Salak, V. Miskovic, E. Dudrova, E. Rudnayova, Powder Metallurgy International **6**, 128 (1974).
[9] I. M. Zakirov – Rolling with coated elastic cylinder, Masinostroenie, Moskow, (1985), (in russian).
[10] A. Palfalvi, I. Vida-Simiti, I. Chicinaş, L. Szabo, I. Magyorosi, Powder Metallurgy International **4**, 16 (1988).
[11] Keishi, Gotoh, Powder Technology, **20**(2), 257 (1978).

*Corresponding author: ivida@personal.ro